Application of alumoxane nanoparticles as precursors for 3D alumina features

RYAN LOSCUTOVA, ANDREW R. BARRON*
Department of Chemistry, Department of Mechanical Engineering and Materials Science, Richard E Smalley Institute for Nanoscale Science and Technology, Rice University, Texas, Houston 77005, USA
E-mail: arb@rice.edu; url www.rice.edu/barron

Published online: 12 April 2006

Acetate- and methoxy(ethoxyethoxy)acetate-functionalized alumina nanoparticles (A-alumoxane and MEEA-alumoxane, respectively) have been investigated as processable, water soluble precursors to 3-dimensional (3D) ceramic features. The ceramic features were formed by slip-casting aqueous solutions of the alumoxanes into polydimethylsiloxane molds, into which negative images of the desired features were molded. The features ranged from 50 to 450 μm in width and approximately 70 μm in depth. Drying the aqueous solution, and removal from the molds revealed free-standing thin film 'green bodies' on which are the positive images of the features, which upon firing (1200°C) resulted in their conversion to α-alumina. The formation of the 'green body' upon drying of the alumoxane solution and its sintering to ceramic was studied with regard to shrinkage and cracking. Ceramic 3D features formed from A-alumoxane faithfully reproduced the dimensions of the green body. However, shrinkage and cracking during the drying phase was observed. In contrast, MEEA-alumoxane was found to remain 'plastic' in its green body state, allowing for the retention of large features, but the shrinkage upon sintering (due to MEEA-alumoxane's lower ceramic yield) was often accompanied by cracking of features. Physical mixtures of the two alumoxanes were investigated to determine optimum conditions for the controlled fabrication of ceramic features. The best combination of properties was obtained for a 2:1 mixture of A-alumoxane and MEEA-alumoxane. If metal-doped MEEA-alumoxane was employed, the appropriate aluminate ceramic was formed. Green body and ceramic samples were characterized by SEM, XRD, BET, and Vickers hardness measurements.

1. Introduction

MicroElectroMechanical Systems (MEMS) or, more simply, micromachines, are complex machines with micron feature sizes that are aimed at merge sensing, actuating, and computing, in order to realize new systems that bring enhanced levels of perception, control, and performance [1, 2]. MEMS to date have evolved from the fabrication technologies used for semiconductor devices, and thus, are traditionally fabricated from Si, SiO_2, SiC, and Si_3N_4 [3–5]. Such materials generally find use in high temperature, oxidizing, or otherwise harsh chemical environments. For example, MEMS features formed in borosilicon carbonitride have been demonstrated to be stable in air up to 1050°C [6]. However, these materials can undergo substantial shrinkage during pyrolysis, in excess of 30%. Further difficulties to MEMS fabrication with materials such as silicon carbide and silicon nitride are the propensity to undergo phase transformations, difficulties in machining, and degradation above 1400°C. Oxide-based ceramics, such as alumina, do not suffer from these drawbacks. Furthermore, the corrosive resistance and hardness make alumina ideal for the fabrication of protective coatings and three-dimensional MEMS type features and structures.

The desire to expand the choice of potential materials that may be employed to structural ceramics, high temperature stable or catalytic active materials, and materials with specific surface functionalization (pK_a and surface wetting), has led to a number of alternative chemical approaches to MEMS fabrication, including the use of

*Author to whom all correspondence should be addressed.
0022-2461
DOI: 10.1007/s10853-005-5343-8

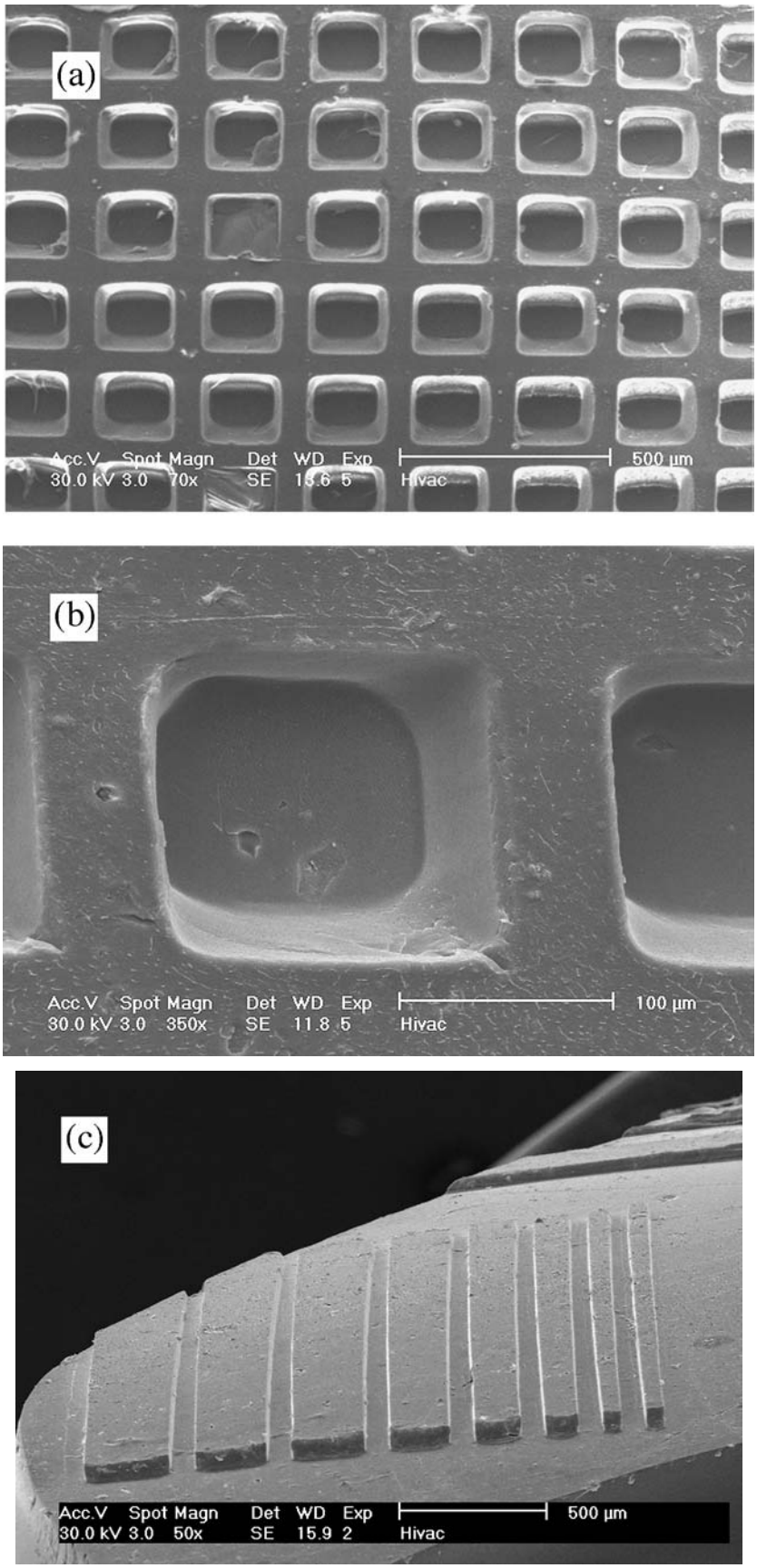

Figure 1 SEM images of ceramic features derived from A-alumoxane: (a) and (b) an array of wells and (c) parallel channels.

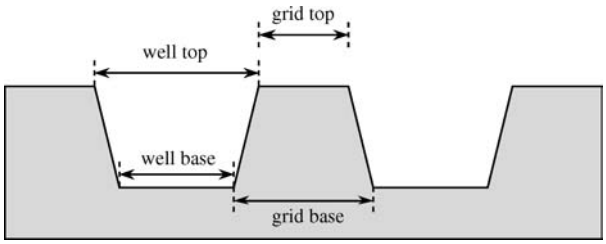

Figure 2 Schematic representation of measurements made on wells.

polymeric precursors [1]. Alumina and metal aluminates [7] have been neglected in MEMS fabrication, despite their desirable physical and chemical properties [8, 9]. Alumina containing MEMS have been fabricated using pre-formed alumina powders [10, 11] and anodic aluminum oxide [12]. Previous workers [13–15] have shown that infiltration of polymeric precursors into polydimethylsiloxane (PDMS) molds formed through 'soft' lithography allow for the rapid screening of various chemical compositions. This fabrication approach should be applicable to sol-gel as well as other 'precursor' methodologies.

We have previously reported that chemically functionalized alumina nanoparticles (alumoxanes) may be processed from aqueous solution to provide conformal coatings [17, 18] or as surface repair agents [19]. Furthermore, doping of the nanoparticles allows for the facile formation of a wide range of aluminates [20]. In the present work, we have investigated the suitability of alumoxane nanoparticles for the fabrication of simple 3D structures. In particular, our interest is in how the surface substituents (carboxylate groups) affect the ability to create specific shapes.

2. Experimental procedure

2.1. Alumoxane choice and synthesis

Two alumoxanes were chosen for the study, acetate- and methoxy(ethoxyethoxy)acetate-functionalized alumina nanoparticles (A-alumoxane and MEEA-alumoxane, respectively). A-alumoxane has an average particle size of 30 nm and has a ceramic yield of 60% that should result in minimum shrinkage upon firing. In contrast, MEEA- has a lower ceramic yield (37%) but remains 'plastic' upon drying to a green body. Both alumoxanes are water-soluble, form alumina upon firing to 460°C and are formed by the reaction of boehmite with the appropriate carboxylic acid [21].

Research grade boehmite (Catapal-B) was provided by Sasol. Acetic acid and methoxy(ethoxy ethoxy)acetic acid (Fisher Scientific and Fluka, respectively) were used without further purification. The A-alumoxane and MEEA-alumoxane were synthesized according to previously reported literature procedures [21, 22]. Y-doped and Ca-doped MEEA-alumoxanes was prepared by previously published methods [23, 24] using $Y(acac)_3$ and $Ca(acac)_2$, respectively (Strem Chemical).

Stock (50 wt.%) solutions of A-alumoxane and MEEA-alumoxane were made by stirring the powder in water at room temperature, and allowing to set overnight into a gel. The gels were homogenized by stirring an hour after blending, to prevent clumping. For mixed blends of A-alumoxane and MEEA-alumoxanes, the ratios of alumoxane and water were always kept at 50 wt.%, to ensure a densely setting gel. Mixed alumoxane gels were prepared by the addition of the appropriate quantity of each alumoxane to water resulting in a 50 wt.% solution of alumoxane. Mixtures with 100, 80, 66, 50, 33, 20, and 0 wt percentages of A-alumoxane were prepared. To form large green bodies of thickness greater than 4 mm, 20 wt.% solutions of alumoxane were made. The same percentages of mixed alumoxanes were used as for the thin film green bodies.

2.2. Feature selection and 3D-feature fabrication

Three types of features were investigated with particular reference to the ability of the alumoxanes to reproduce

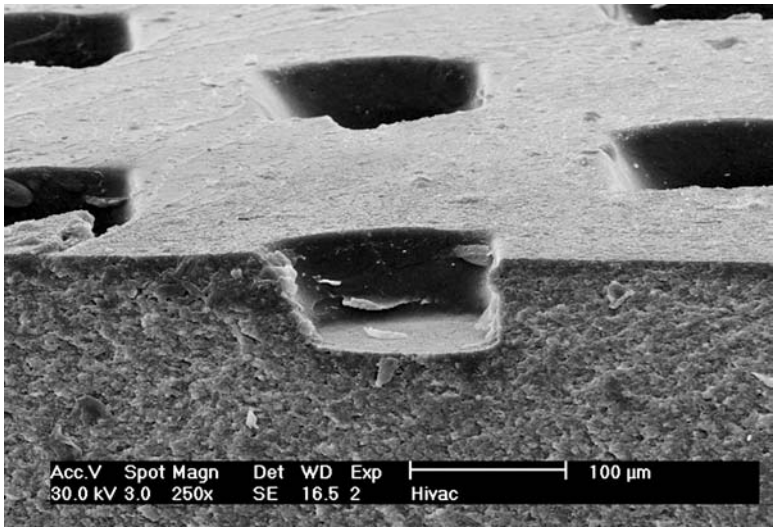

Figure 3 SEM image of ceramic features illustrating deformation during setting process.

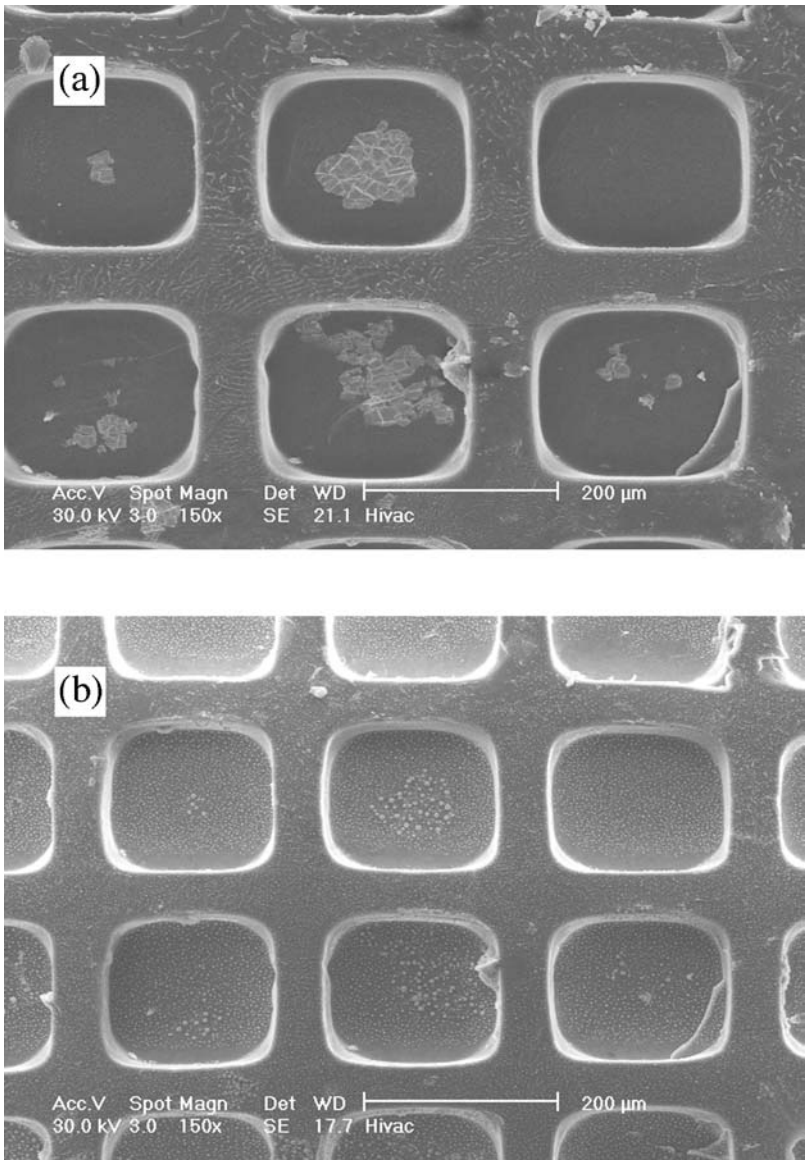

Figure 4 SEM images of A-alumoxane thin film (a) green body, and (b) fired ceramic.

feature sizes and aspect ratios. An array of wells (200×200 μm), with inter-well wall widths (50 μm), was used to determine the effect of the alumoxanes on a repeated pattern and the variation of sidewall shrinkage. Large letters, "ARB", (500 μm font with a 100 μm brush stroke) were used to determine the effect of the alumoxanes on the reproduction of large features. Finally, a series of parallel bars with various widths (300–50 μm) and inter-channel spacing (50 μm) was used to determine the effect of the alumoxanes on the reproduction of uniform sidewalls.

The polydimethylsiloxane (PDMS) molds were fabricated from Sylgard 184 (Dow Corning) prepolymer. A two-dimensional representation of the desired image was drafted using MacDraw Pro, and then photographed with 35 mm high-resolution film. The film negatives reproduced line widths ranging from 0.5 to 200 μm. Negative photoresist (SU-8, MicroChem Corporation) was spuncoat onto a silicon wafer substrate, baked, and subsequently exposed to UV light (<300 nm) through the film negatives. Following development, the wafers were trimmed to size, and suspended within the PDMS prepolymer, that was allowed to cure for 2 h at 70°C, and subsequently hardened by heating to 170°C for 3 h. The silicon wafer was carefully carved out of the nascent "deep dish" mold. The negative 3D image was thus reproduced onto the bottom of the mold surface.

The PDMS mold was cleaned with 0.5% alconox, and rinsed with deionized H_2O. The appropriate gel was carefully spread over the features of the mold with a small spatula. An optical microscope (50×) was used to inspect the gels, to ensure complete surface wetting and filling of the void spaces. Gels were set to heights of 0.5 to 1 mm. The films were then allowed to dry at room temperature for 1–5 days. After drying, the nascent films or large green bodies were carefully peeled from the base

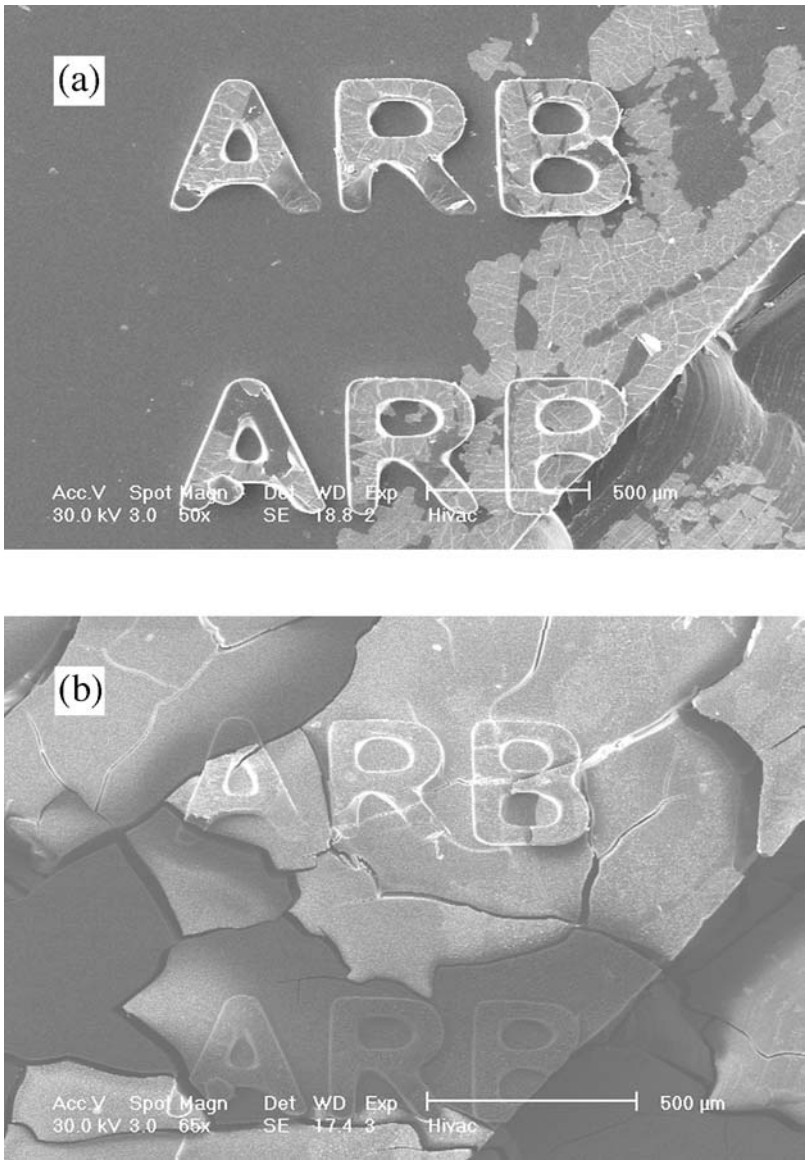

Figure 5 SEM images of MEEA-alumoxane (a) green body, illustrating excellent feature reproduction, and (b) final ceramic, showing extensive cracking incurred during firing.

of the molds. The films or green bodies were then sintered in an oven (Carbolite model RHF 1500) according to a ramp rate determined from TGA decompositions of the A- and MEEA-alumoxanes, which showed mass loss to be complete after 500°C. Both films and green bodies were ramped to 100°C at 0.5°C. min^{-1}, held for 1 h., further ramped to 475°C at 0.375°C. min^{-1}, and finally to 1200°C at 0.725°C. min^{-1}, and held for 6 h.

2.3. Characterization

Surface area analysis was performed on Coulter SA 3100 BET analyzer using N_2 gas adsorption. The samples were outgassed under nitrogen for 1 h at 200°C before analysis. Micro-indention testing was performed on a Micromet microhardness tester. Load weights varied with the sample. The hardness was determined by inserting the load weight and the area of indention into the Vicker's equation: $H_v = 1.85444(P/d^2)$ where P is the load in Kg and d^2 is the area of indention in mm^2. Powder X-ray diffraction was performed on a Siemens Diffractometer.

SEM images were obtained using a Phillips model XL-30 at an accelerating voltage of 30 KeV. Samples were attached to an aluminum specimen mount (Electron Microscopy Sciences) or onto carbon or copper tape affixed to a specimen mount. Before imaging, insulating samples were sputter coated (Plasma Sciences CRC 100) with a thin layer of either gold or chromium to prevent charging.

3. Results and discussion

3.1. A-Alumoxane

Green bodies formed from A-alumoxane with a large sample thickness (4 mm) exhibit significant cracking during drying. The overall body has significant shrinkage that

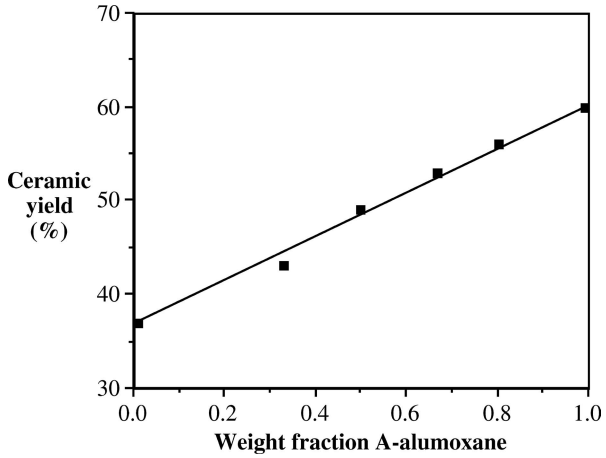

Figure 6 Plot of ceramic yield as a function of the composition of the green body (MEEA-alumoxane:A-alumoxane).

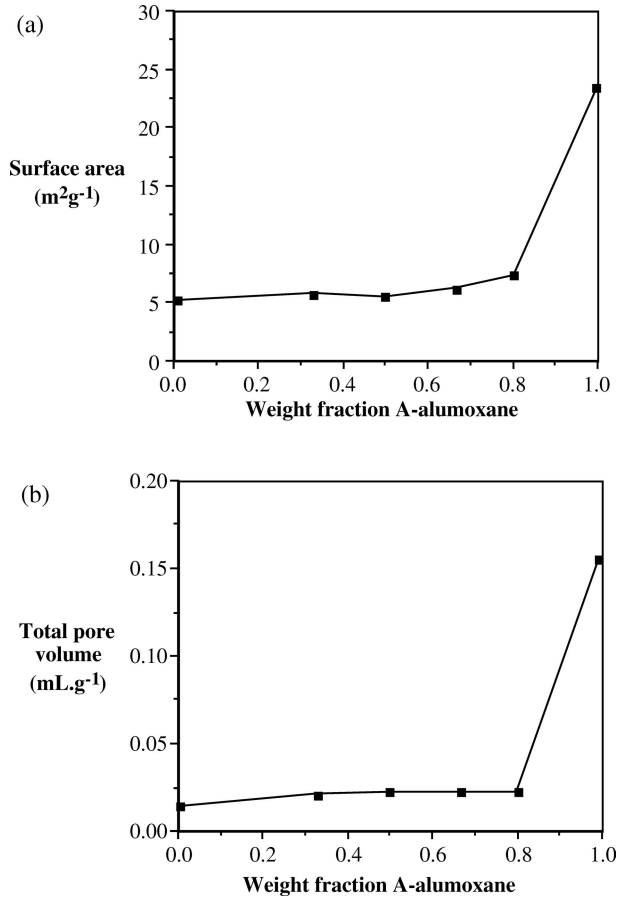

Figure 7 Plots of (a) surface area and (b) total pore volume for ceramic bodies fired at 1200°C as a function of the composition of the green body (MEEA-alumoxane:A-alumoxane).

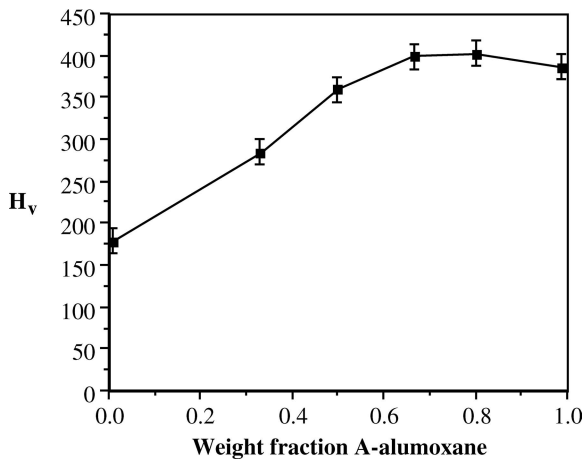

Figure 8 Plot of the Vickers hardness for ceramic bodies fired at 1200°C as a function of the composition of the green body (MEEA-alumoxane:A-alumoxane).

results in the body pulling-away from the molds leaving non-parallel sides to many of the features (see below). Less cracking and feature asymmetry is observed when the sample thickness is reduced below 1 mm.

Firing the A-alumoxane green body to ceramic and sintering to 1200°C for 6 h. results in the formation of an alumina body essentially identical in shape and features to that of the green body (Fig. 1). Any asymmetry observed in the green body (for samples where the base of the body is thicker than 1 mm) is carried over to the ceramic. No additional cracks are observed during this process (although as may be expected defects present in the green body are carried over to the ceramic body). Overall shrinkage is low, consistent with the high ceramic yield of A-alumoxane.

As may be seen from Fig. 1a the array of wells is replicated with a high degree of reproducibility. However, despite the high ceramic yield, the shrinkage upon sintering the green body is large (28%). Furthermore, the distribution of values varies widely (15–41%). A consideration of the variation between the top and base of the wells and the grid between the wells (see Fig. 2) shows a variation from 20% to 30%. The sidewalls of each well are non-parallel, resulting in the base of each well being significantly smaller than its top. This variation is readily seen in Fig. 1b where all four sidewalls may be seen for wells even when viewed from directly above. A view of the wells in cross-section highlights this effect (Fig. 3). Based upon a comparison with the molds, it appears that the significant shrinkage that occurs as the A-alumoxane dries to the green body results in its being squeezed away from the mold by the features. The extent of the distortion is dependent on the position of the 3D feature within the macroscopic body. We propose that the feature deformation appears to be a consequence of the body size (in particular its thickness). Therefore, we have investigated the fabrication of thinner samples by limiting the amount of A-alumoxane placed into the molds. In regard to larger features, such as parallel bars (Fig. 1c) this distortion has less of an effect upon the overall appearance of the features.

Fig. 4 shows SEM images of the green and associated ceramic body of the array of wells, for a thin film sample (sample thickness = ca. 1 mm). It is clear from this comparison that all of the features are faithfully

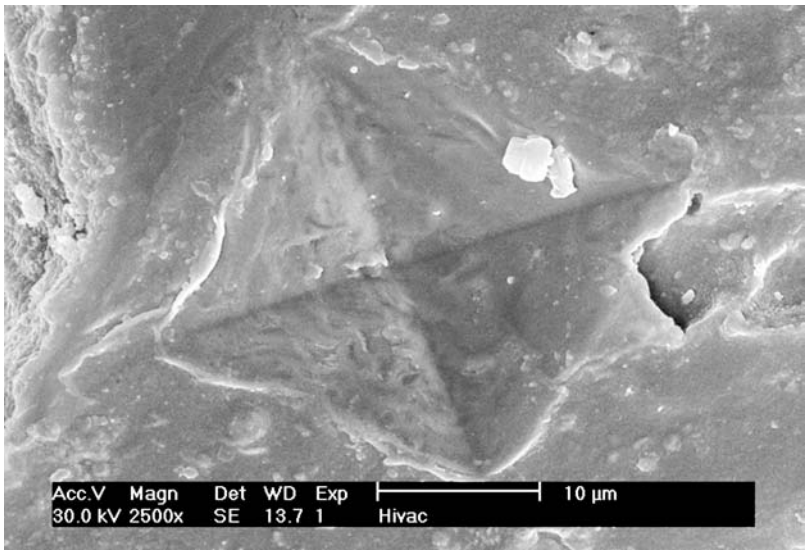

Figure 9 SEM image of the surface of a 3D alumina feature formed from a 2:3 MEEA-alumoxane:A-alumoxane green body sintered to 1200°C for 6 h. showing effects of micro-indentation.

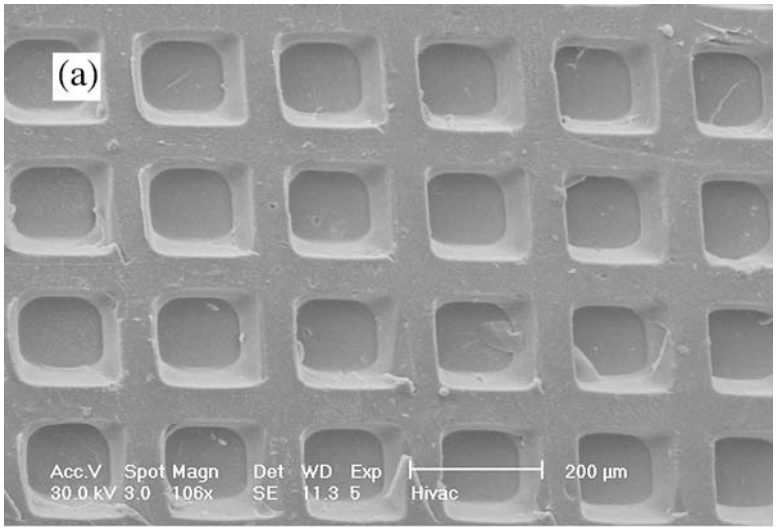

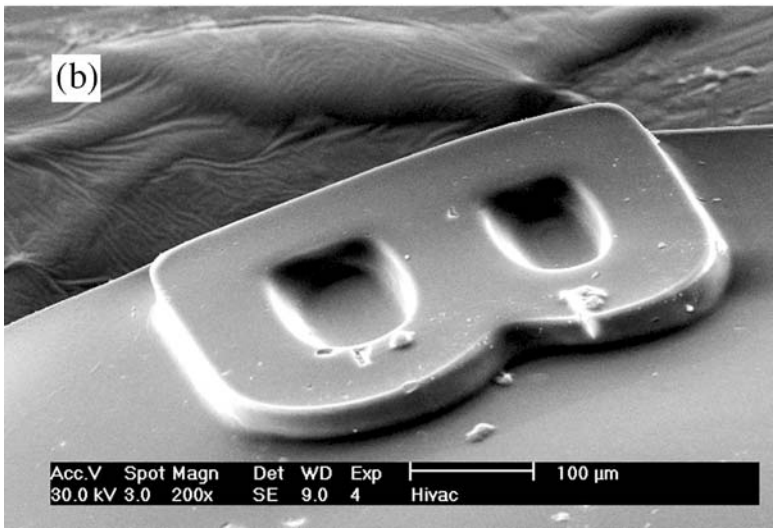

Figure 10 SEM images of typical 3D ceramic features prepared from alumoxane blends: (a) an array of wells prepared from 1:4 MEEA-alumoxane:A-alumoxane, and (b) individual "B" prepared from 1:1 MEEA-alumoxane:A-alumoxane.

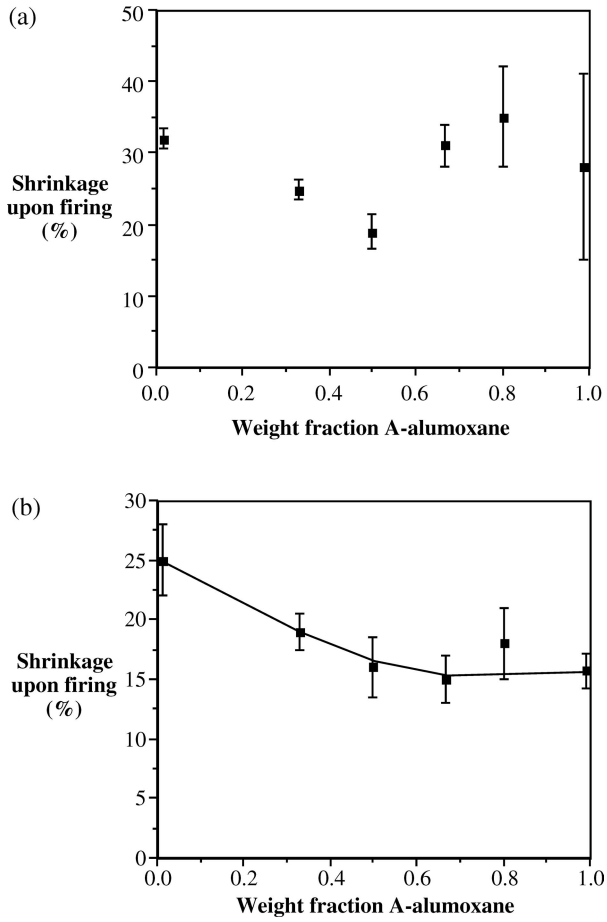

Figure 11 Plots of the average shrinkage in feature size as a function of green body composition for (a) thick and (b) thin film samples.

reproduced, including the defect in the sidewall of the central well at the bottom of the image, and the base of the well to its right. The picture frames also visually illustrate the amount of bulk shrinkage incurred during the firing process. Unlike thicker samples where significant strain is present, the average feature shrinkage (18%) is very small (consistent with the higher ceramic yield of A-alumoxane), but the deviation is also very small (4%). In fact, the range of shrinkage for A-alumoxane thin films is the same as for thicker films formed from MEEA-alumoxane (see below), where the higher plasticity of MEEA-alumoxane preserves feature fidelity—at a cost of reduced ceramic strength.

It is also clear from Fig. 4 that the sidewalls of the wells are much closer to parallel for thin film samples. The deviation from parallel (i.e., the difference between the well base and top, *c.f.* Fig. 2) is *ca.* 8% for both the green body and the fired ceramic. Thus, not only is the strain diminished during drying, but also no additional distortion is carried over to the ceramic features.

In summary, while the high ceramic yield of A-alumoxane allows for minimal shrinkage of 3D features during sintering, the exact replication of any feature is highly dependent on the drying of the A-alumoxane solution to the green body. With low weight-percent loadings (ca. 5%), the shrinkage during drying can cause the green bodies to show significant cracking and/or deformation. Deformation effects may be limited with decreased thickness of the body, or higher weight-percent loadings of alumoxane.

3.2. MEEA-alumoxane

In contrast to the fragile green bodies formed from A-alumoxane, the green bodies formed from MEEA-alumoxane are free from cracking and exhibit a high degree of feature reproduction (Fig. 5a). It appears that MEEA-alumoxane remains plastic in its green body state, allowing for the retention of large features during drying. Certainly, the MEEA-alumoxane green bodies are flexible as compared to the brittle A-alumoxane green bodies.

MEEA-alumoxane has a significantly lower ceramic yield than A-alumoxane, and therefore significant shrinkage of the 3D features occurs during sintering (32%). The range of shrinkage upon sintering of MEEA-alumoxane derived features is narrow ($< \pm 2\%$). Unfortunately, the MEEA-alumoxane derived ceramic bodies show extensive cracking (Fig. 5b), even for thin film samples. Attempts to retain macroscopic structure by variation of the sintering and cycling rates were not successful. Based upon our studies the cracking is less influenced by thermal history and cyclying rates than on the ceramic yield associated with the alumoxane precursor.

In summary, the plastic texture of MEEA-alumoxane allows for large green bodies to be formed, and for maximal fidelity of feature reproduction. The shrinkage range is less susceptible to sample size, and deformation effects are negligible. However, the low ceramic yield of the MEEA-alumoxane results in a higher shrinkage than for

TABLE I Relative properties of ceramics derived from MEEA-alumoxanes

Alumoxane	Ceramic yield (%)	Surface area ($m^2\ g^{-1}$)	Pore volume ($mL\ g^{-1}$)	Vickers hardness ($Kg\ mm^{-2}$)
MEEA-alumoxane	37	5.249	0.0143	176
Ca-doped MEEA-alumoxane[a]	45	9.779	0.0838	[c]
Y-doped MEEA- alumoxane[b]	43	8.402	0.1094	183

[a]The calcium dopant level is sufficient to form $CaAl1_2O_{19}$ (hibonite) upon sintering.
[b]The yttrium dopant level is sufficient to form $Y_3Al_5O_{12}$ (YAG) upon sintering.
[c]Sample too brittle to obtain meaningful measurement.

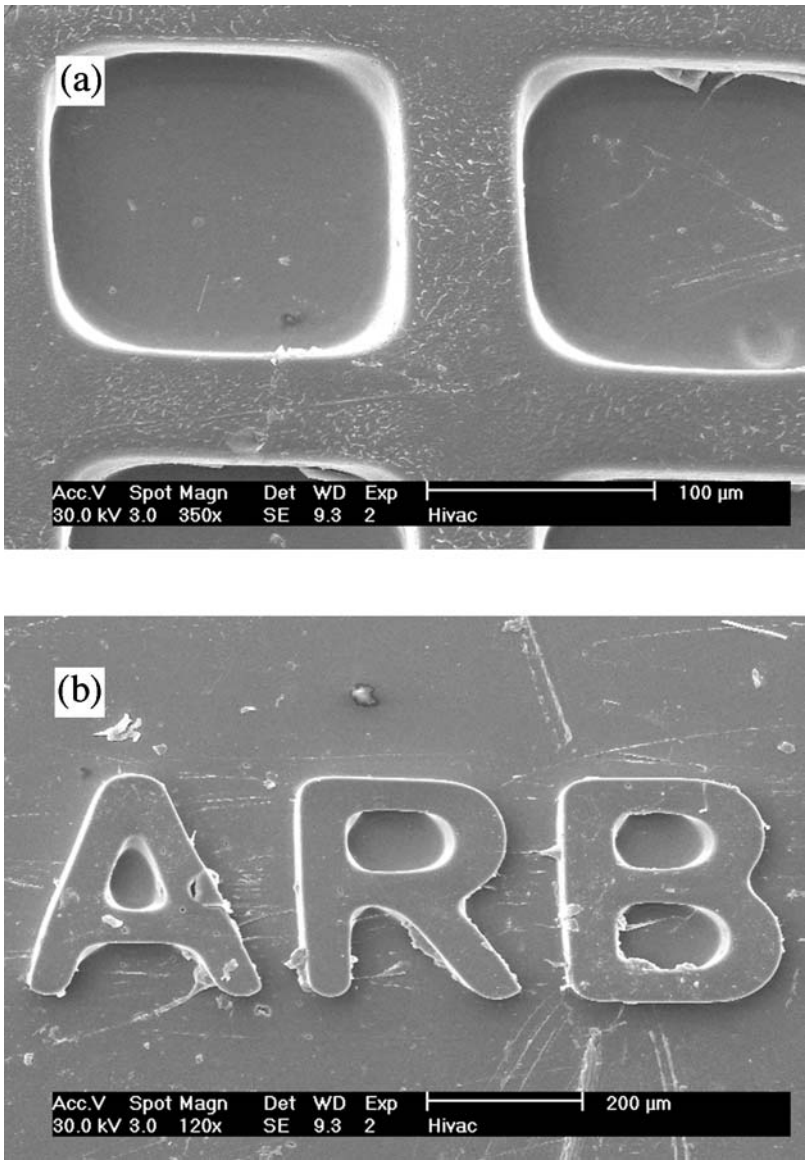

Figure 12 SEM images of a 2:1 blend of A-alumoxane and yttrium-doped MEEA-alumoxane, resulting in yttrium aluminum garnet wells with vertical sidewalls (a), and raised letters (b).

optimized A-alumoxane samples, as well as a deteriorated final ceramic.

3.3. Alumoxane blends

Based upon the forgoing, MEEA-alumoxane allows for faithful reproduction of a green body from a mold with isotropic shrinkage and retention of structure over a large sample (8 cm), however, upon sintering the ceramic bodies are of poor quality. In contrast, A-alumoxane does not produce ideal green bodies, but they are converted faithfully (along with their defects) into ceramic features. In order to determine whether blending the alumoxanes could provide both optimum green body strength and the formation of ceramic features of high definition, physical mixtures of the two alumoxanes were investigated.

Prior to investigating the formation of 3D features the effects of the green body on physical properties should be considered. As may be seen from Fig. 6 there is the expected linear relationship between ceramic yield and composition of the green body. The surface area and total pore volume of ceramic bodies prepared from blends of MEEA-alumoxane and A-alumoxane sintered under identical conditions is shown in Fig. 7. In neither case is there is a linear relationship between the values for the individual alumoxanes, i.e., the resulting ceramic is not a simple mixture of ceramics formed from the component precursors. Both properties appear dominated by the presence of the MEEA-alumoxane, even at levels as low as 1:4 MEEA-alumoxane:A-alumoxane.

Interestingly, a plot of the Vickers hardness as a function of green body composition (Fig. 8) shows that the hardness of the resulting ceramic is dominated by the presence of A-alumoxane. Only when the fraction of MEEA-alumoxane in the green body is greater than 50% is there any significant decrease in hardness. Unlike the

porosity of the features, this observation offers the possibility of obtaining 3D features with optimum hardness. There is no cracking or grain dislodgement after microindentation testing (e.g., Fig. 9) suggesting that the 3D features are of uniform fine grain size. This is confirmed by XRD measurements that show the crystallite size to be 16 ± 1 nm for all samples.

Fig. 10 shows typical examples of 3D ceramic features prepared from blends of MEEA-alumoxane and A-alumoxane. As expected, an increase in MEEA-alumoxane content allows for more stable green bodies. In addition, samples with more than 40% A-alumoxane show a distinct decrease in cracking upon sintering.

Shown in Fig. 11a is a plot of the average feature size shrinkage and range as a function of green body composition for thick samples. As the fraction of A-alumoxane increases the range of feature shrinkage (i.e., feature deformation) increases dramatically, while the average value appears to follow two trends. First, from 0–50% A-alumoxane the shrinkage decreases with increased A-alumoxane content. Second, from 50–100% A-alumoxane, the average shrinkage stays constant, but the range increases. Are these trends explainable? The first trend is expected from a consideration of the relative ceramic yields (Fig. 6). Thus as the ceramic yield increases the shrinkage decreases since less material is lost during sintering. The second trend is at first glance counterintuitive. To understand the second trend we must consider the increase in the range of shrinkage in a given sample. The large range of shrinkage for a given feature in A-alumoxane rich green bodies is due to a significant anisotropy (distortion) of the features (see above). Thus, while the A-alumoxane-rich derived bodies remain intact there is significant strain exerted on the features, causing distortion as shown in Fig. 3. As discussed above for A-alumoxane, it would be expected that if thin film structures were formed (with a concomitant decrease in strain during drying), A-alumoxane rich derived ceramics would indeed provide a more faithful replication of their green bodies. This is indeed observed. As shown in Fig. 11b the average feature size shrinkage as a function of green body composition for thin samples follows a well defined trend. Thus, we conclude therefore that in samples where bulk strain is minimized the inherent range of shrinkage is about 3–4%, while the absolute shrinkage actually correlates very well with ceramic yield.

3.4. Doped alumoxanes

We have previously demonstrated that alumoxanes undergo a metal exchange that allows for the facile synthesis of doped alumina and metal aluminates upon sintering [20, 23, 24]. The reaction of an alumoxane with an appropriate metal acetylacetonate complex results in the formation of the doped alumoxane and the aluminum acetylacetonate complex; i.e., a one-for-one metal exchange occurs between the alumoxane nanoparticle and the soluble metal complex. In this study we have chosen calcium and yttrium doping that allow for the formation of $CaAl_{12}O_{19}$ (hibonite) and $Y_3Al_5O_{12}$ (YAG), respectively .

As may be seen from Table I, there is a small increase in the ceramic yield for both Ca- and Y-doped MEEA-alumoxanes as compared to the virgin parent, MEEA-alumoxane. This increase is expected based upon the increased mass of the dopant metal in comparison with aluminum. However, despite the small increase in ceramic yield, the surface area and pore volume of the ceramics thus formed are much greater for the doped alumoxanes than for the virgin MEEA-alumoxane sample. This alteration in porosity is a function of the phase formed upon sintering.

In order to ascertain if the dopants significantly alter the replication of 3D features we have investigated their formation using a 2:1 blend of A-alumoxane and the metal-doped MEEA-alumoxane. As may be seen from Fig. 12 the substitution of MEEA-alumoxane with Y-doped MEEA-alumoxane results in the formation of robust ceramic pieces with near isotropic shrinkage. The shrinkage for the grid of wells (Fig. 12a) upon sintering the green bodies is identical to that observed for the analogous 2:1 blend of A-alumoxane and the MEEA-alumoxane (see above). Thus, the presence of dopant and the formation of an aluminate phase have no effect on the replication of the 3D features.

4. Conclusions

We have shown the ability to make micron-sized 3D ceramic features with alumoxane-based alumina nanoparticles. Varying the blend of alumoxanes alters the quality of the final ceramic, ranging from very high image fidelity in green pieces high in MEEA content, to very strong and robust ceramic pieces high in A-alumoxane, with low instances of cracking. Altering the weight percent loadings of nanoparticles allows for less water loss during the setting process, resulting in reduced feature deformation. In addition, mixed-metal doped alumoxanes produce features from alternative phases of alumina such as hibonite or YAG.

Acknowledgments

Financial support for this work was provided by the Robert A. Welch Foundation, and the National Science Foundation.

References

1. S. M. ALLAMEH, *J. Mater. Sci.* **38** (2003) 4115.
2. T. E. BUCHHEIT, S. J. GLASS, J. R. SULLIVAN, S. S. MANI, D. A. LAVAN, T. A. FRIEDMANN and R. Janek, *ibid.* **38** (2003) 4081.
3. A. T. LOPES and M. N. P. CARRENO, *J. Non-Cryst. Solids.* **788** (2004) 338.
4. D.-C. LIM, H.-G. JEE, J. W. KIM, J.-S. MOON, S.-B. LEE, S. S. CHOI and J.-H. BOO, *Thin Solid Films* **459** (2004) 7.

5. O. M. JADAAN, N. N. NEMETH, J. BAGDAHN and W. N. SHARPE JR., *J. Mater. Sci.* **38** (2003) 4087.
6. H. YANG, P. DESCHATELETS, S. T. BRITTAIN and G. M. WHITESIDES, *Adv. Mater.* **13** (2001) 54.
7. R. KUBO, Y. YOSHINO, K. INOUE, T. MAKINO and S. ARAI, *Mater. Res. Soc., Symp. Proc.* **657** (2001) 1.
8. E. L. COURTRIGHT, *Ceram. Eng. Sci. Proc.* **12** (1991) 1725.
9. C. K. NARULA, J. E. ALLISON, D. R. BAUER and H. S. GANDHI, *Chem. Mater.* **8** (1996) 984.
10. S. CHAROENMECHAIKUL and D. E. LUZZI, *Mater. Res. Soc., Symp. Proc.* **546** (1999) 183.
11. T. WANG, M. SORRELL, K. KELLY and E. MA, *Proc. SPIE-The Interna. Soc. Opti. Engng.* **3512** (1998) 344.
12. K. I., DELENDIK and O. L. VOITIK, *ibid.* **4592** (2001) 355.
13. Y. XIA and G. M. WHITESIDES, *Angew. Chem. Int. Ed.* **37** (1998) 550.
14. B. ZHENG, J. D. TICE and R. F. ISMAGILOV, *Adv. Mater.* **15** (2004) 1365.
15. M. GEISSLER and Y. XIA, *ibid.* **15** (2004) 1249.
16. S. JEON, E. MENARD, J. U. PARK, J. MARIA, M. MEITL, J. ZAUMSEIL and J. A. ROGERS, *ibid.* **15** (2004) 1369.
17. R. L. CALLENDER and A. R. BARRON, *J. Mater. Sci.* **36** (2001) 4977.
18. *Idem. ibid.* **15** (2000) 2228.
19. K. A. DEFRIEND and A. R. BARRON, *ibid.* **37** (2002) 2909.
20. R. L. CALLENDER and A. R. BARRON, *J. Am. Ceram. Soc.* **83** (2000) 1777.
21. R. L. CALLENDER, C. J. HARLAN, N. M. SHAPIRO, C. D. JONES, D. L. CALLAHAN, M. R. WIESNER, R. COOK and A. R. BARRON, *Chem. Mater.* **9** (1997) 2418.
22. C. C. LANDRY, N. PAPPÈ, M. R. MASON, A. W. APBLETT, A. N. TYLER, A. N. MACINNES and A. R. BARRON, *J. Mater. Chem.* **5** (1995) 331.
23. A. KAREIVA, C. J. HARLAN, D. B. MACQUEEN, R. COOK and A. R. BARRON, *Chem. Mater.* **8** (1996) 2331.
24. C. J. HARLAN, A. KAREIVA, D. B. MACQUEEN, R. COOK and A. R. BARRON, *Adv. Mater.* **9** (1997) 68.

Received 3 November 2004
and accepted 12 July 2005